J Biol Phys (2007) 33:357–370
DOI 10.1007/s10867-008-9059-2

ORIGINAL PAPER

Influence of Distal Residue B10 on CO Dynamics in Myoglobin and Neuroglobin

Karin Nienhaus · G. Ulrich Nienhaus

Received: 14 October 2007 / Accepted: 8 February 2008 /
Published online: 5 April 2008

Abstract For many years, myoglobin has served as a paradigm for structure–function studies in proteins. Ligand binding and migration within myoglobin has been studied in great detail by crystallography and spectroscopy, showing that gaseous ligands such as O_2, CO, and NO not only bind to the heme iron but may also reside transiently in three internal ligand docking sites, the primary docking site B and secondary sites C and D. These sites affect ligand association and dissociation in specific ways. Neuroglobin is another vertebrate heme protein that also binds small ligands. Ligand migration pathways in neuroglobin have not yet been elucidated. Here, we have used Fourier transform infrared temperature derivative spectroscopy at cryogenic temperatures to compare the influence of the side chain volume of amino acid residue B10 on ligand migration to and rebinding from docking sites in myoglobin and neuroglobin.

Keywords Fourier transform infrared spectroscopy · Ligand migration · Myoglobin · Neuroglobin · Temperature derivative spectroscopy

1 Introduction

Hemoglobins (Hbs) are abundant in all kingdoms of life [1, 2]. Their physiological function involves reversible binding of small ligands such as O_2, NO, or CO at the central iron of a heme prosthetic group enclosed by the polypeptide chain in its characteristic α-helical 'globin' fold. The functional properties of the heme group are markedly influenced by amino acids in its vicinity, especially by amino acid residues B10 and E7 near the active site. These residues may, for example, stabilize heme-bound ligands by hydrogen bonding. Notwithstanding a few exceptions, e.g., Asian elephant myoglobin (Mb) [3], vertebrate oxygen storage and transport proteins utilize the leucine B10/histidine E7 (LeuB10/HisE7)

K. Nienhaus (✉) · G. U. Nienhaus
Institute of Biophysics, University of Ulm, Albert-Einstein-Allee 11, 89081 Ulm, Germany
e-mail: Karin.Nienhaus@uni-ulm.de

G. U. Nienhaus
Department of Physics, University of Illinois at Urbana-Champaign, 1110 West Green Street, Urbana, IL 61801, USA

pair, which appears optimally suited for reversible binding of O_2 [4, 5] (all secondary structure assignments indicate the corresponding positions in helices A–H of Mb). Other members of the globin protein family carry the tyrosine B10/glutamine E7 (TyrB10/GlnE7) combination at the active site; among these are the truncated Hbs [6]. The O_2 affinities in this subset of globins are for the most part too high for reversible binding, as required by an O_2-transport protein, due to the strong stabilization of the heme-bound O_2 by both GlnE7 and TyrB10. However, the TyrB10/GlnE7 pair is highly effective in NO scavenging and detoxification [7]. Hbs in which the heme iron is hexacoordinated by the axial ligands HisE7 and HisF8 in the absence of an exogenous ligand have been found in plants; they have phenylalanine B10/histidine E7 (PheB10/HisE7) in their distal pocket [8]. In Rice HbI, PheB10 was shown to facilitate stable O_2 coordination to the ferrous form and to promote ligand binding to the ferric species [9]. Structurally homologous globins, neuroglobin (Ngb) and cytoglobin, are present in vertebrates [10, 11]. Their physiological functions are still under investigation.

In the field of biological physics, Mb has played a central role as a model system for the investigation of protein structural dynamics [12–18]. Detailed ligand-binding studies on Mb with both spectroscopic [19–23] and crystallographic [24–30] techniques have disclosed that the amino acids at positions E7 and B10 play important roles in regulating ligand access to the heme iron. No permanent channel exists in the molecular structure of Mb that connects the active site to the outside, but an outward movement of the HisE7 imidazole side chain may transiently open a pathway through which ligands may enter or exit the distal heme cavity [31, 32]. After entering the protein from the solvent, the ligand may shuttle among the primary docking site B and secondary docking sites C and D before either binding to the heme iron (from site B) or exiting again into the solvent when the HisE7 gate is open (Fig. 1a). Ligands bound at the heme iron (site A) may dissociate and become transiently trapped at site B [25, 27, 30]. From there, they can either rebind, escape into the solvent, or migrate to the secondary sites C and D, which are cavities in the protein that were initially found to bind Xe atoms and, therefore, are also denoted as Xe4 and Xe1 cavities [33]. From site D on the proximal side of the heme, ligands first return to the distal pocket before they can exit the protein [28]. At 290 K, they can stay unbound inside Mb for up to 1 μs. The distal heme pocket has been likened to a baseball glove that catches the

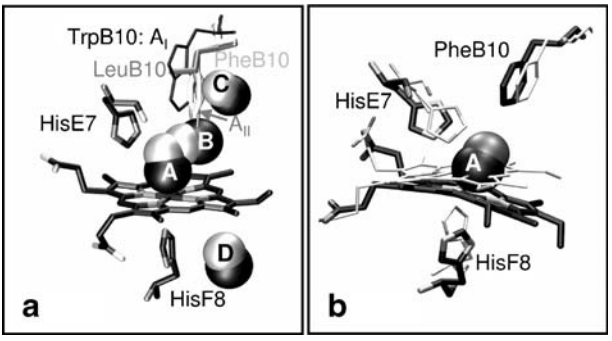

Fig. 1 Active-site structures of **a** Mb and **b** Ngb. **a** The heme and residues HisE7 and HisF8 are represented by *stick models*. PheB10 (pdb accession code 1JDO [72]) is *added in white*; the A_I (1DO4 [26]) and A_{II} (1DO3 [26]) conformations of TrpB10 are indicated. The CO ligand in van der Waals representation is depicted at the binding site A, the primary docking site B (1ABS [27]), and secondary sites C (1DO4 [26]) and D (1DO3 [26]). **b** The ferric form of Ngb (1Q1F [43]) is shown as a *white stick model*. CO-ligated Ngb (1W92 [44]) is shown in *gray*, with the CO in van der Waals representation

incoming ligands at the primary docking site B [23]. The Mb mutant Leu(B10)Phe demonstrates how structural variations of the distal pocket can have large functional effects (Fig. 1a). In this mutant, site B is partially blocked by the aromatic side chain so that ligands that dissociate from the heme iron are reflected right back into the binding site. As a consequence, the dissociation rate coefficient is decreased ~10-fold, resulting in an unusually high O_2 affinity [23, 34]. Moreover, incoming ligands are deflected back into the solvent, which causes a decrease in the association rate coefficient. Time-resolved X-ray structure analysis has revealed that this mutation also affects the residence times of the ligand at the docking sites [29, 35].

The effects of the aromatic amino acids tryptophan (Leu(B10)Trp [36, 37]) and tyrosine (in YQR (Leu(B10)Tyr/His(E7)Gln/Val(E10)Arg) [38]) at position B10 on the overall ligand-binding kinetics of Mb are similar. The three aromatic B10 mutants display an interesting structural heterogeneity of their side chains. The indole side chain of TrpB10 can adopt two conformations, A_I and A_{II} (Fig. 1a) [26, 28]. A_I dominates at cryogenic temperatures; upon increasing the temperature, the A_{II} population increases at the expense of A_I [37, 39]. In contrast, both TyrB10 and PheB10 are found in only one orientation. The TyrB10 side chain prefers the A_I-like position [40], whereas PheB10 is seen in the A_{II}-like conformation (Fig. 1a) [29].

In comparison with Mb, much less is known about the structural details of exogenous ligand binding in Ngb [41, 42]. It involves an additional step, the dissociation of the distal HisE7 side chain to make the sixth coordination site available for an external ligand. Subsequently, the heme plane slides deeper into the protein, as revealed by X-ray crystallography (Fig. 1b) [43, 44]. Ligand escape is extremely fast; CO molecules spend less than 30 ns unbound inside the wild-type protein after photodissociation at ambient temperature [41]. Nevertheless, a significant fraction rebinds geminately on even faster timescales, which suggests that PheB10 performs a function similar to that in Mb mutant Leu(B10)Phe, that is, to occlude the primary docking site. To create a more Mb-like distal pocket with a B site potentially better suited for ligand capture, we have replaced PheB10 by LeuB10 in Ngb. By comparison with the corresponding variants of Mb, we aim to obtain information on the structural determinants of ligand migration and binding in Ngb.

Fourier transform infrared (FTIR) spectroscopy in the stretching bands of heme-bound and photodissociated CO has proven to be a superb tool to study ligand migration and binding in heme proteins [21, 26, 37, 45]. The strong infrared absorption of the bound CO ligand is highly sensitive to the local electric field at the binding site and indicates structural heterogeneity. Multiple active-site conformations had been inferred from the CO stretching spectrum of wild-type MbCO [46] long before their individual structures were revealed by X-ray crystallography [47, 48]. The CO ligand can be photodissociated from the iron at cryogenic temperatures and can migrate to trapping sites B, C, and D, where it gives rise to characteristic stretching bands [21, 37]. Typically, the CO molecule can assume two opposite orientations in each docking site [49], and the vibrational Stark effect yields a doublet of infrared (IR) bands in the presence of a local electric field [50–52].

2 Materials and Methods

2.1 Sample Preparation

Wild-type and Leu(B10)Phe sperm whale Mb were expressed in *Escherichia coli* strain Tb1 and purified as described [53]. Site-directed mutagenesis of murine Ngb was performed

using the Quikchange mutagenesis kit (Stratagene Europe, Amsterdam). Cysteine-depleted Ngb (C55S/C120S), which is termed wild-type Ngb in the following, was used as template. Custom-designed primers were ordered from MWG (MWG-Biotech GmbH, Ebersberg, Germany). The Ngb proteins were expressed in *E. coli* and purified according to [41]. For the IR experiments, lyophilized protein was dissolved at a concentration of ~15 mM in cryosolvent (75% glycerol/25% potassium phosphate buffer (*v*/*v*), pH 8), stirred under a CO atmosphere and reduced with a twofold molar excess of sodium dithionite solution.

2.2 Fourier Transform Infrared Spectroscopy

Transmission spectra were collected in the mid-IR between 1,800 and 2,400 cm^{-1} with a resolution of 2 cm^{-1}, using a FTIR spectrometer (IFS 66v/S, Bruker, Karlsruhe, Germany) equipped with an InSb detector. Sample loading and cryogenic equipment have been described previously [20, 54].

The solid lines in Fig. 2 show photolysis difference spectra of the samples in the regions of the IR stretching bands of the heme-bound (1,900–2,000 cm^{-1}) and photodissociated CO (2,100–2,160 cm^{-1}), calculated from transmission spectra taken before and after photolysis for 1 s at 4 K. For better comparison, the difference spectra were scaled to identical amplitudes. Note that the integrated absorption is more than 20 times smaller in the CO photoproduct bands than in the bands of the heme-bound form. The bands with negative absorption near 1,950 cm^{-1} indicate the heme-bound CO missing after photolysis. Each band represents one so-called 'taxonomic' or 'A' substate characterized by a unique heme pocket structure [14]. The different stretching frequencies arise from electrostatic interactions of the CO dipole with different local electric fields at the binding site. At ambient temperature, Mb molecules fluctuate between the different substates on nanosecond time scales [55, 56]. Below the dynamical transition temperature of ~180 K, however, large-scale motions are arrested [13, 57] so that each molecule is frozen into one of the A substate conformations. Upon photodissociation at low temperatures, the CO cannot escape from the protein but can only migrate within, and different electrostatic interactions also give rise to multiple bands of the photolyzed CO due to trapping at different transient sites within the protein or different orientations at a particular site [50–52]. As these photoproduct bands emerge upon photodissociation, they are plotted with positive amplitudes in Fig. 2. In addition to 1-s photolysis at 4 K, the samples were also cooled under steady illumination from 160 to 4 K (ramp rate 0.3 K/min), which is a convenient method to screen for transient docking sites [19, 58].

2.3 Temperature Derivative Spectroscopy

To assign photoproduct bands to particular docking sites, the rebinding properties of the photoproduct species were determined using temperature derivative spectroscopy (TDS), an experimental protocol designed to investigate thermally activated rate processes with distributed enthalpy barriers [19, 59, 60]. Such distributions are inferred from the nonexponential rebinding of ligands in heme and other proteins at cryogenic temperatures; they are a result of conformational heterogeneity [12, 61]. The sample is photodissociated prior to the TDS experiment, and the measurement is started at the lowest temperature desired. FTIR transmittance spectra, $I(\nu, T)$, are taken every 1 K while increasing the sample temperature T at a rate of 0.3 K/min. FTIR absorbance difference spectra, $A(\nu, T)$, are calculated from transmittance spectra at successive temperatures, which approximates the

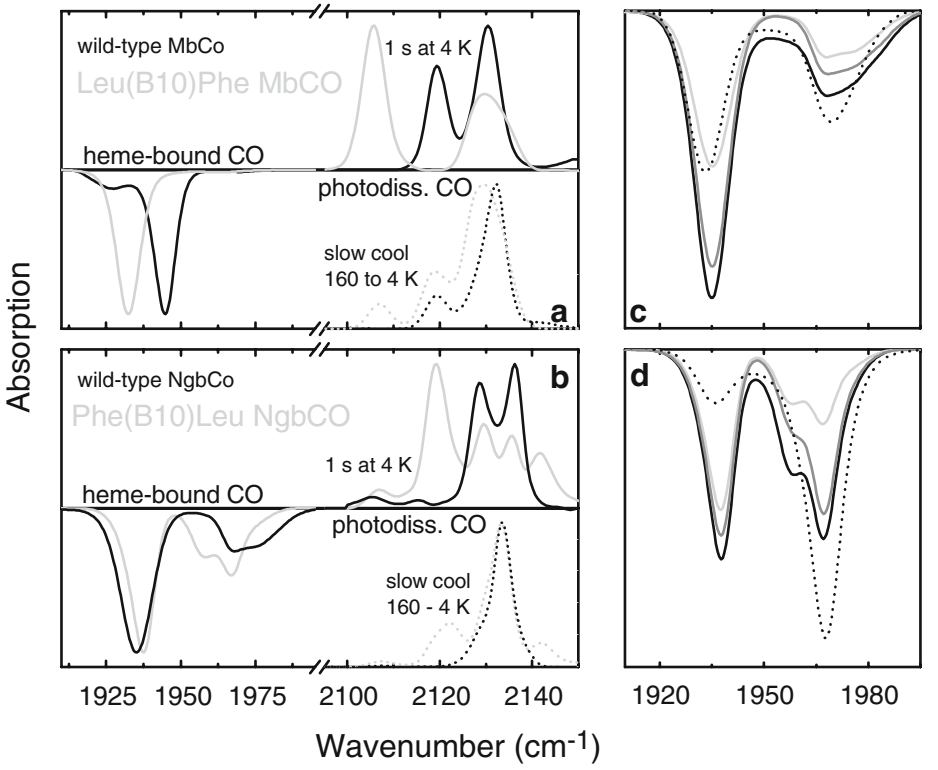

Fig. 2 FTIR difference spectra of MbCO and NgbCO samples in the spectral regions of heme-bound and photodissociated CO inside the proteins (pH ~7). Photolysis difference spectra of **a** wild-type MbCO (*black*), Leu(B10)Phe MbCO (*gray*), and **b** wild-type NgbCO (*black*), Phe(B10)Leu NgbCO (*gray*) were calculated from transmission spectra collected before and after 1-s illumination at 4 K (*solid lines*) and slow cool illumination from 160 to 4 K (*dotted lines*). The spectra were scaled to identical peak amplitudes. FTIR absorbance difference spectra of **c** wild-type NgbCO and **d** Phe(B10)Leu NgbCO reveal the photolysis yields. *Solid lines* 4-K spectra of total heme-bound CO (*black*), photolyzed by 1-s illumination at 4 K (*light gray*) and photolyzed during slow cooling (*gray*). *Dotted lines* 290-K spectra calculated from NgbCO and metNgb transmission spectra; they reveal the overall heme-bound CO at 290 K

derivative. For ligand rebinding, the change in spectral area is taken proportional to the fraction of ligands that rebind during acquisition of two successive spectra. However, absorption changes can also arise from ligand dynamics within a docking site [50, 51], ligand migration to different docking sites [21, 62] and conformational changes of the protein [63]. The temperature ramp protocol ensures that rebinding occurs sequentially with respect to the temperature at which the different processes become activated on the time scale of the experiment. TDS is a so-called 'rate-window method' which shifts all processes sequentially into a rate (or time) window that can be controlled by the temperature ramp rate and is typically ~0.01 s^{-1} (100 s) [59]. TDS data are usually displayed as contour plots of the absorbance change on a surface spanned by the wave-number and temperature axes (Figs. 3 and 4). The absorbance changes can also be integrated along the wave-number axis and plotted against the temperature axis to display the rebinding behavior in a condensed fashion (Fig. 5).

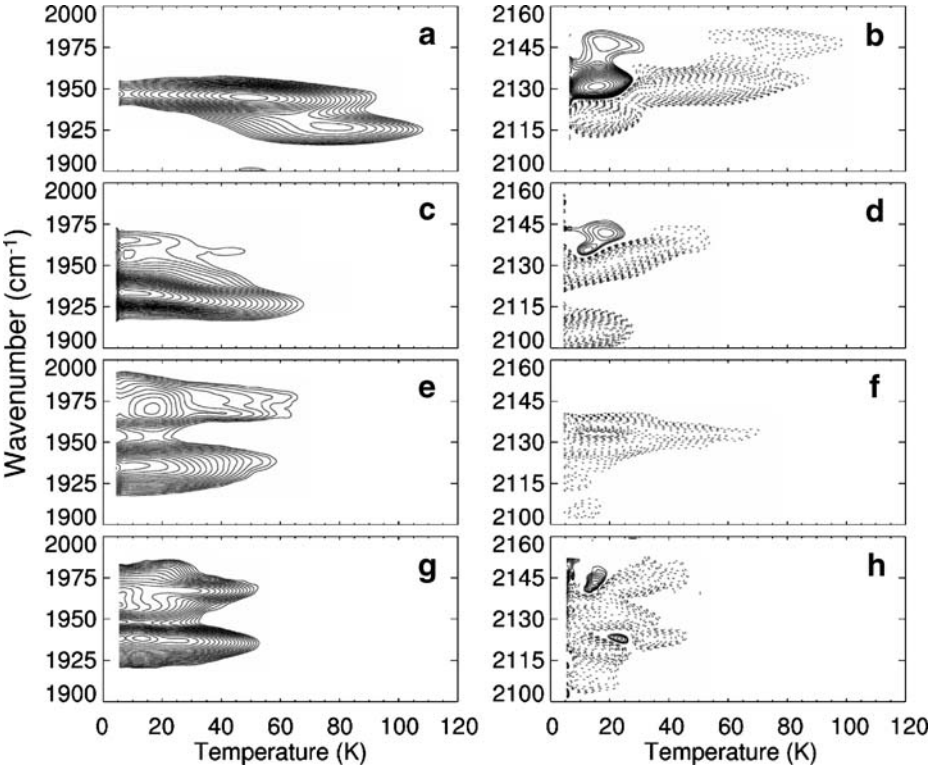

Fig. 3 TDS contour maps of **a**, **b** wild-type MbCO; **c**, **d** Leu(B10)Phe MbCO; **e**, **f** wild-type NgbCO; and **g**, **h** Phe(B10)Leu NgbCO obtained after 1-s illumination at 4 K. *Left column* absorption changes in the bands of bound CO. *Right column* absorption changes in the photoproduct bands. *Solid lines* indicate an absorption increase; *dotted lines* indicate a decrease in absorption. Contours are spaced logarithmically

3 Results and Discussion

3.1 Structural Heterogeneity in the CO-bound State

The infrared stretching bands of heme-bound CO are known to be excellent reporters of structural heterogeneity in globins due to their exquisite sensitivity to local electric fields that are created by amino acid residues surrounding the active site [50, 52, 64]. At pH 7.3, the CO stretching spectrum of wild-type MbCO is governed by two bands, A_1 at 1,945 cm^{-1} and A_3 at 1,930 cm^{-1} (Fig. 2a, black line). In both conformations, HisE7 is neutral, and the hydrogen on the Nε atom forms a hydrogen bond with the ligand oxygen. The high resolution X-ray structure indicates that the positive partial charge of the HisE7-NεH is positioned slightly closer to the bound ligand in the A_3 conformation than in A_1 [48], thereby shifting the stretching band to a lower frequency [65, 66]. At low pH, a third band emerges at 1,965 cm^{-1}. It represents the so-called A_0 conformation, in which the HisE7 side chain is protonated (pK=4.5 [67]) and rotated toward the solvent [47].

In Leu(B10)Phe MbCO (pH 7.4), the dominant stretching band of the heme-bound CO is shifted to 1,935 cm^{-1}, which indicates an A_3-like conformation (Fig. 2a, gray line). In

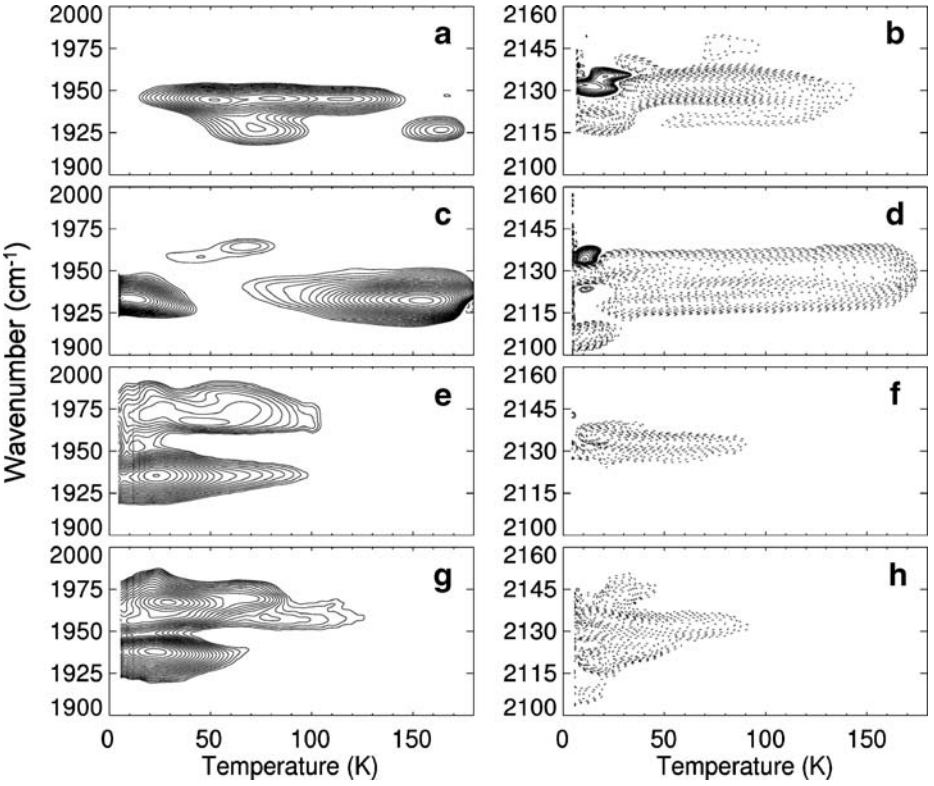

Fig. 4 TDS contour maps of **a**, **b** wild-type MbCO; **c**, **d** Leu(B10)Phe MbCO; **e**, **f** wild-type NgbCO; and **g**, **h** Phe(B10)Leu NgbCO obtained after slow cooling from 160 to 4 K under steady illumination. *Left column* absorption changes in the bands of bound CO. *Right column* absorption changes in the photoproduct bands. *Solid lines* indicate an absorption increase; *dotted lines* indicate a decrease in absorption. Contours are spaced logarithmically

addition to His-NεH, a positive partial charge may also be contributed by the edge of the aromatic PheB10 ring. A very small, rather broad A_0 band is resolved at 1,962 cm^{-1}. The A_1/A_3 heterogeneity is no longer present.

Wild-type NgbCO displays three stretching bands of heme-bound CO at pH 7.2 (Fig. 2b, solid black line), A_1 peaking at 1,935 cm^{-1}, A_0 (1,968 cm^{-1}) and A_2 (1,978 cm^{-1}; note that the peak positions differ slightly from those reported in [68] because we have worked with cysteine-substituted proteins in the present study). The dominant band, which we had earlier denoted by A_1 [41], is actually related to the A_3 band that is present in MbCO mutants that also carry an aromatic residue at position B10 [36, 62]. In the A_0 conformation, the HisE7 side chain is protonated and turned away from the bound ligand [42], which renders the binding site less polar [68]. The structural determinants governing the high-frequency A_2 band are less clear [68]. The high frequency suggests that a negative partial charge is present near the CO oxygen, and two possible conformations may be discussed for this arrangement [68]: (1) The π-electron system of PheB10 interacts with the bound ligand. The Phe(B10)Leu mutation would abolish this interaction. (2) A neutral HisE7 with a protonated Nδ points its non-bonding electron pair on Nε at the bound ligand.

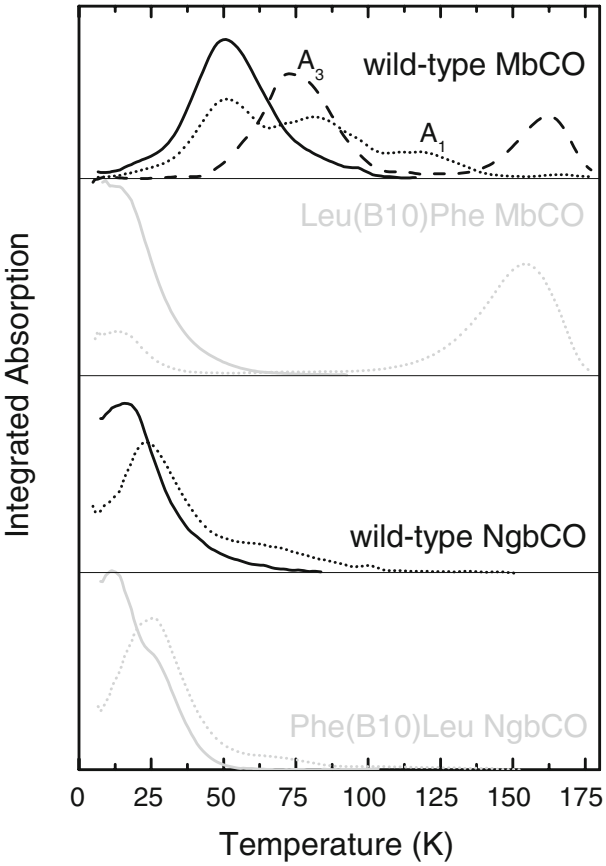

Fig. 5 Integrated absorption changes calculated from the TDS contour maps in the left columns of Fig. 3 (*solid lines*) and Fig. 4 (*dotted lines*). The absorption changes in the wild-type MbCO substates A_1 and A_3 after slow-cool illumination are plotted separately

This conformation is physiologically of particular relevance because only this Nδ tautomer can form the hexa-coordinate ferrous species after dissociation of the exogenous ligand. A combination of both effects is also conceivable: tautomerism of HisE7 may induce reorientation of PheB10 which in turn could result in the electrostatic interaction between its π-electron system and the bound ligand.

Phe(B10)Leu NgbCO (pH 7.0) also displays three active-site conformations. The dominant A_1 band has shifted from 1,935 to 1,938 cm^{-1}; the decreased line width indicates a more homogeneous conformation (Fig. 2b, solid gray line). The comparatively small frequency shift reflects a smaller change in protein–ligand interactions than in MbCO, which is consistent with the more spacious heme pocket of NgbCO. As in the wild-type protein, there are also two high-frequency bands. We suggest that A_0 stays at 1,968 cm^{-1} and thus represents a species with minimal interaction between the CO and the distal heme pocket environment also in the mutant. The third band resides at 1,959 cm^{-1}. We also denote it by A_2 for simplicity, but it cannot be assigned unambiguously. Removal of the PheB10 side chain interaction should remove the negative partial charge and thus eliminate the high-frequency band corresponding to the A_2 conformation of wild-type NgbCO at 1,978 cm^{-1}, which is indeed observed. The frequency of 1,959 cm^{-1} suggests a fairly weak interaction of the CO with a positive partial charge, likely from the HisE7 imidazole.

However, water in the distal heme pocket could also be responsible for the observed band shift.

3.2 Intermediate Ligand Docking Sites in Myoglobin

The photoproduct spectra in Fig. 2 display multiple bands that cannot be assigned to CO ligands in specific intermediate docking sites without further information. TDS experiments are useful to observe rebinding from the photoproduct states and to disperse the different processes according to temperature. The contour maps obtained after 1-s illumination and slow-cool illumination from 160–4 K are compiled in Figs. 3 and 4, respectively. To simplify the comparison of the rebinding patterns after the two illumination protocols, we have plotted the integrated absorption changes in Fig. 5 (solid lines, 1 s illumination; dotted lines, slow cool illumination).

After 1-s illumination of wild-type MbCO at 4 K, all ligands are photolyzed. They are found trapped at the primary docking site B on top of pyrrole C [25, 27, 30]. Opposite orientations of the ligands in the B site of A_1 molecules are represented by the photoproduct bands at 2,119 and 2,131 cm^{-1} [21, 46]. In the A_3 conformation, ligands at site B also give rise to a doublet of bands, but only the band at 2,149 cm^{-1} is spectrally separated (Fig. 2a). Non-equilibrium 2D-IR exchange spectroscopy experiments on mutant Val(E11)Tyr MbCO have indicated that the stretching band representing the opposite orientation in A_3 is occluded by the 2,119-cm^{-1} band of A_1 [69]. Reorientation at the B site is thermally activated at ~20 K, as indicated by the concomitant solid and dotted contours at ~20 K in the photoproduct TDS map (Fig. 3b). Rebinding in A_1 peaks at ~48 K, as seen from the contours in Fig. 3a, which corresponds to a barrier of ~10 kJ/mol [56]. Ligands in A_3 encounter markedly higher enthalpy barriers (~18 kJ/mol [56]) and thus rebind at ~70 K due to the increased steric hindrance by the HisE7 side chain. After extended illumination, site B remains the preferred CO docking site in wild-type MbCO (Figs. 4a and 5). However, significant fractions of ligands in the A_1 conformation are also trapped in sites C (Xe4 cavity) and D (Xe1 cavity), from where they rebind at ~80 and ~125 K [21]. In A_3 molecules, site C is not occupied; rebinding from site D occurs at 160 K [21]. Upon activation of large-scale protein motions, CO ligands in Leu(B10)Trp MbCO crystals can also escape to site D [26, 39].

A comparison of the photolysis difference spectra of wild-type MbCO and Leu(B10)Phe MbCO confirms that the mutation markedly affects the local electric fields at the binding site and the primary docking site (Fig. 2). The photoproduct spectrum of the mutant sample obtained after 1-s illumination displays two features at 2,106 and ~2,130 cm^{-1}. The TDS data indicate that rebinding starts in the mutant already at the lowest temperatures measured (Figs. 3c and 5). The primary docking site does not seem well suited to accommodate the ligands so that they encounter much smaller barriers against rebinding. Moreover, the integrated absorption is not 20 times smaller than that of the heme-bound bands as expected but rather 30 times, indicating that a significant fraction of the photolyzed CO is not trapped at a specific site but gives rise to a broad absorption that cannot be distinguished from the background. As the photoproduct bands at 2,106 and 2,128 cm^{-1} already begin to vanish at 4 K, they may be assigned to CO ligands at site B (Fig. 3d). Small positive contours peaking at 15 K correspond to ligands reorienting in site B [49, 52]. At temperatures >20 K, the contours at ~2,128 cm^{-1} display a drastic shift by more than 10 cm^{-1} towards higher wave numbers with temperature (Fig. 3d). A similar, although less significant, shift is visible in the A state map (Fig. 3c). This phenomenon has been termed ‘kinetic hole burning’ (KHB). It reflects structural heterogeneity and indicates that the same structural

parameter governs both the position of the individual spectral line and the enthalpy barrier for recombination [70, 71]. The pronounced KHB effect in the A and B substates suggests that slight structural changes in the HisE7/PheB10 side chain positions translate into substantial changes in the rebinding enthalpy of this mutant. Another interesting effect visible in the contour map (Fig. 3d) is that some ligands are thermally activated to migrate to an alternative docking site while the TDS experiment is ongoing, as can be seen from the solid contours that peak at 20 K and 2,142 cm^{-1}. These ligands then rebind at ~50 K. A similar migration process has been observed in MbCO mutant YQR and was assigned to migration to and rebinding from the Xe4 cavity [62].

After slow-cool illumination of Leu(B10)Phe MbCO, most of the CO molecules become trapped at a single alternative docking site, and only ~20% remain in site B, as compared to ~50% in wild-type MbCO. This dominant photoproduct site, which is depopulated at ~160 K (Figs. 4c and 5), can be assigned to site D based on several findings: (1) The recombination temperature is comparable to the one for rebinding from site D in A_3 of wild-type MbCO (Fig. 5). (2) The orientation of the PheB10 side chain is similar to that of TrpB10 in the A_{II} conformation of mutant Leu(B10)Trp, where site C is also not occupied (Fig. 1a) [39]. (3) The photoproduct spectrum of this site is identical to that of site D in wild-type MbCO, which is expected because the electric field in the Xe1 cavity on the proximal side of the heme should not be affected by a mutation on the distal site.

In summary, when an aromatic B10 side chain is in the A_I-like conformation, as in YQR or Leu(B10)Trp MbCO (Fig. 1a), the B site is accessible to the ligand, but site C is the preferred ligand trap after photolysis at cryogenic temperatures. The PheB10 side chain in its A_{II}-like conformation occludes the B and C sites but allows for efficient CO trapping in D. Trapping in D in the A_{II} conformation of Leu(B10)Trp MbCO has been confirmed by time-resolved X-ray diffraction experiments at ambient temperature [29]. The significantly prolonged residence time in the D cavity of mutant Leu(B10)Trp has provided evidence that the docking site is located on a migration side path and not on the entry/exit pathway [28].

3.3 Intermediate Ligand Docking Sites in Neuroglobin

Details of ligand migration in Ngb are still scarce. Narrow photoproduct bands are definite proof of well-defined docking sites [41, 68]; however, their physical locations are still not known. It is also difficult to predict putative sites because the protein has a huge internal cavity of ~300 $Å^3$ and a small apolar cavity corresponding to Xe4 in Mb. In the hexacoordinate state, the huge open volume connects the distal and proximal sides of the heme and has a direct connection to the bulk solvent [43]. The tunnel is maintained upon binding of an exogenous ligand; however, its accessibility from the bulk is restricted because of the decreased flexibility of the whole protein [44].

In contrast to MbCO, 1-s illumination of both wild-type and mutant NgbCO at 4 K is not sufficient to keep all ligands photolyzed long enough to detect them in the TDS experiment (Fig. 2c,d). The photolysis yield in wild-type NgbCO amounts to ~50% in each of the substates. In mutant Phe(B10)Leu NgbCO, ~75% of the A_1 substate is photolyzed but only ~40% of A_0 and A_2, suggesting that site B in A_1 molecules has become better suited to trap a ligand. However, even slow cooling the NgbCO samples does not result in complete photolysis, indicating very low barriers against rebinding in Ngb.

After 1-s illumination, wild-type NgbCO shows strong rebinding features already at 4 K (Fig. 3e). The enthalpy barrier distribution for rebinding can be described by a gamma function peaking at 1.1 kJ/mol [68]. In analogy to MbCO, we propose that the two main photoproduct bands at 2,129 and 2,136 cm^{-1} (Fig. 2b) arise from Stark splitting of the CO

band in the local electric field at the primary docking site B of A_1 where the ligands reside in opposite orientations with about equal probability. Rebinding from the photoproduct state represented by the band at 2,129 cm^{-1} peaks at 7 K, whereas most ligands in the other orientation recombine at 20 K; a few migrate to site C at ~25 K (Fig. 3f). After slow cooling of the sample under illumination from 160 to 4 K, ligands rebind from the secondary docking site C which is represented by the photoproduct band at 2,134 cm^{-1} (Fig. 4f). This process is maximal at ~25 K (Fig. 5), which suggests that this site may still be close to the binding site. An additional rebinding process that extends from ~50 to ~100 K might represent recombination from still another docking site D, which is represented by a band at 2,133 cm^{-1} (Fig. 5).

With respect to the integrated absorption changes plotted in Fig. 5, migration and rebinding seem very similar for the NgbCO mutant sample: rebinding at the lowest temperatures from a primary docking site, rebinding from a second site at ~25 K, and from a third site producing the tail around 70 K. As compared to Mb, the effect of the Phe(B10) Leu replacement on the inner barriers is thus only minor in Ngb. The photoproduct spectrum obtained after 1-s illumination, however, reveals an increased manifold of photoproduct states as compared to the wild-type protein (Fig. 2b), which requires a fit with at least five Gaussian bands at 2,106, 2,119, 2,129, 2,136, and 2,142 cm^{-1} to describe the spectrum. The rather complicated photoproduct map (Fig. 3h) indicates that additional photoproduct bands are hidden in the difference spectrum and only emerge in the TDS contour map. The latter fact is seen from the concomitant solid and dotted contours at particular temperatures that represent ligand reorientation or migration. After slow-cool illumination, the TDS features of the wild-type NgbCO map are essentially retained (Fig. 4f,h) and supplemented by new contours peaking at 2,119, 2,123, and 2,142 cm^{-1}. This result implies that the secondary sites are unchanged in the mutant sample. The smaller LeuB10 side chain apparently allows the CO ligands to sample new sites, which may suggest that these are located close to this residue.

4 Conclusions

In Mb, a voluminous B10 side chain constitutes a steric barrier between the binding site and secondary sites Xe4 and Xe1, resulting in efficient ligand trapping at cryogenic temperatures and a decrease of the association rate under physiological conditions [23]. The effect is most pronounced in mutant Leu(B10)Trp, which has the slowest room temperature on-rate observed so far [23, 37, 39]. In contrast, in Ngb, the volume of the B10 residue does not markedly affect the barriers against ligand migration and rebinding at cryogenic temperatures. However, the FTIR spectra of NgbCO and its Phe(B10)Leu mutant at 290 K are markedly different from those at 4 K (dashed lines in Fig. 2c,d). In the wild-type protein, the majority of protein molecules are in the A_1 conformation, whereas in the mutant, the strong band at 1,968 cm^{-1} indicates that by far the most proteins are in the open A_0 conformation, leading to faster ligand association to the pentacoordinate heme species and faster dissociation of HisE7 from the ferrous iron (data not shown). Hence, PheB10 in Ngb is important for stabilizing the closed conformation, in which the HisE7 side chain is inside the distal pocket.

Acknowledgements This work was supported by the Deutsche Forschungsgemeinschaft (grant Ni 291/3) and the Fonds der Chemischen Industrie. We thank Uwe Theilen for expression and purification of the recombinant proteins used in this study.

References

1. Hardison, R.C.: A brief history of hemoglobins: plant, animal, protist, and bacteria. Proc. Natl. Acad. Sci. U. S. A. **93**, 5675–5679 (1996)
2. Weber, R.E., Vinogradov, S.N.: Nonvertebrate hemoglobins: functions and molecular adaptations. Physiol. Rev. **81**, 569–628 (2001)
3. Bisig, D.A., Di Iorio, E.E., Diederichs, K., Winterhalter, K.H., Piontek, K.: Crystal structure of Asian elephant (Elephas maximus) cyano-metmyoglobin at 1.78-A resolution. Phe29(B10) accounts for its unusual ligand binding properties. J. Biol. Chem. **270**, 20754–20762 (1995)
4. Olson, J.S., Mathews, A.J., Rohlfs, R.J., Springer, B.A., Egeberg, K.D., Sligar, S.G., Tame, J., Renaud, J.P., Nagai, K.: The role of the distal histidine in myoglobin and haemoglobin. Nature **336**, 265–266 (1988)
5. Olson, J.S., Phillips Jr., G.N.: Kinetic pathways and barriers for ligand binding to myoglobin. J. Biol. Chem. **271**, 17593–17596 (1996)
6. Wittenberg, J.B., Bolognesi, M., Wittenberg, B.A., Guertin, M.: Truncated hemoglobins: a new family of hemoglobins widely distributed in bacteria, unicellular eukaryotes, and plants. J. Biol. Chem. **277**, 871–874 (2002)
7. Gardner, P.R., Gardner, A.M., Martin, L.A., Salzman, A.L.: Nitric oxide dioxygenase: an enzymic function for flavohemoglobin. Proc. Natl. Acad. Sci. U. S. A. **95**, 10378–10383 (1998)
8. Arredondo-Peter, R., Hargrove, M.S., Moran, J.F., Sarath, G., Klucas, R.V.: Plant hemoglobins. Plant Physiol. **118**, 1121–1125 (1998)
9. Smagghe, B.J., Kundu, S., Hoy, J.A., Halder, P., Weiland, T.R., Savage, A., Venugopal, A., Goodman, M., Premer, S., Hargrove, M.S.: Role of phenylalanine B10 in plant nonsymbiotic hemoglobins. Biochemistry **45**, 9735–9745 (2006)
10. Burmester, T., Weich, B., Reinhardt, S., Hankeln, T.: A vertebrate globin expressed in the brain. Nature **407**, 520–523 (2000)
11. Burmester, T., Ebner, B., Weich, B., Hankeln, T.: Cytoglobin: a novel globin type ubiquitously expressed in vertebrate tissues. Mol. Biol. Evol. **19**, 416–421 (2002)
12. Austin, R.H., Beeson, K.W., Eisenstein, L., Frauenfelder, H., Gunsalus, I.C.: Dynamics of ligand binding to myoglobin. Biochemistry **14**, 5355–5373 (1975)
13. Nienhaus, G.U., Heinzl, J., Huenges, E., Parak, F.: Protein crystal dynamics studied by time-resolved analysis of X-ray diffuse scattering. Nature **338**, 665–666 (1989)
14. Frauenfelder, H., Nienhaus, G.U., Johnson, J.B.: Rate processes in proteins. Ber. Bunsenges. Phys. Chem. **95**, 272–278 (1991)
15. Parak, F.G., Nienhaus, G.U.: Myoglobin, a paradigm in the study of protein dynamics. Chem. Phys. Chem. **3**, 249–254 (2002)
16. Samuni, U., Dantsker, D., Roche, C.J., Friedman, J.M.: Ligand recombination and a hierarchy of solvent slaved dynamics: the origin of kinetic phases in hemeproteins. Gene **398**, 234–248 (2007)
17. Parak, F., Frolov, E.N., Mössbauer, R.L., Goldanskii, V.I.: Dynamics of metmyoglobin crystals investigated by nuclear gamma resonance absorption. J. Mol. Biol. **145**, 825–833 (1981)
18. Parak, F., Knapp, E.W., Kucheida, D.: Protein dynamics. Mössbauer spectroscopy on deoxymyoglobin crystals. J. Mol. Biol. **161**, 177–194 (1982)
19. Nienhaus, G.U., Mourant, J.R., Chu, K., Frauenfelder, H.: Ligand binding to heme proteins: the effect of light on ligand binding in myoglobin. Biochemistry **33**, 13413–13430 (1994)
20. Nienhaus, G.U., Nienhaus, K.: Infrared study of carbon monoxide migration among internal cavities of myoglobin mutant L29W. J. Biol. Phys. **28**, 163–172 (2002)
21. Nienhaus, K., Deng, P., Kriegl, J.M., Nienhaus, G.U.: Structural dynamics of myoglobin: The effect of internal cavities on ligand migration and binding. Biochemistry **42**, 9647–9658 (2003)
22. Scott, E.E., Gibson, Q.H.: Ligand migration in sperm whale myoglobin. Biochemistry **36**, 11909–11917 (1997)
23. Scott, E.E., Gibson, Q.H., Olson, J.S.: Mapping the pathways for O_2 entry into and exit from myoglobin. J. Biol. Chem. **276**, 5177–5188 (2001)
24. Bourgeois, D., Vallone, B., Schotte, F., Arcovito, A., Miele, A.E., Sciara, G., Wulff, M., Anfinrud, P., Brunori, M.: Complex landscape of protein structural dynamics unveiled by nanosecond Laue crystallography. Proc. Natl. Acad. Sci. U. S. A. **100**, 8704–8709 (2003)
25. Hartmann, H., Zinser, S., Komninos, P., Schneider, R.T., Nienhaus, G.U., Parak, F.: X-ray structure determination of a metastable state of carbonmonoxy myoglobin after photodissociation. Proc. Natl. Acad. Sci. U. S. A. **93**, 7013–7016 (1996)
26. Ostermann, A., Waschipky, R., Parak, F.G., Nienhaus, G.U.: Ligand binding and conformational motions in myoglobin. Nature **404**, 205–208 (2000)

27. Schlichting, I., Berendzen, J., Phillips Jr., G.N., Sweet, R.M.: Crystal structure of photolysed carbonmonoxy-myoglobin. Nature **371**, 808–812 (1994)
28. Schmidt, M., Nienhaus, K., Pahl, R., Krasselt, A., Anderson, S., Parak, F., Nienhaus, G.U., Srajer, V.: Ligand migration pathway and protein dynamics in myoglobin: a time-resolved crystallographic study on L29W MbCO. Proc. Natl. Acad. Sci. U. S. A. **102**, 11704–11709 (2005)
29. Schotte, F., Lim, M., Jackson, T.A., Smirnov, A.V., Soman, J., Olson, J.S., Phillips Jr., G.N., Wulff, M., Anfinrud, P.A.: Watching a protein as it functions with 150-ps time-resolved X-ray crystallography. Science **300**, 1944–1947 (2003)
30. Teng, T.Y., Srajer, V., Moffat, K.: Photolysis-induced structural changes in single crystals of carbonmonoxy myoglobin at 40 K. Nat. Struct. Biol. **1**, 701–705 (1994)
31. Perutz, M.F.: Myoglobin and haemoglobin: role of distal residues in reactions with haem ligands. Trends Biochem. Sci. **14**, 42–44 (1989)
32. Johnson, K.A., Olson, J.S., Phillips Jr., G.N.: Structure of myoglobin-ethyl isocyanide. Histidine as a swinging door for ligand entry. J. Mol. Biol. **207**, 459–463 (1989)
33. Tilton Jr., R.F., Kuntz Jr., I.D., Petsko, G.A.: Cavities in proteins: structure of a metmyoglobin-xenon complex solved to 1.9 Å. Biochemistry **23**, 2849–2857 (1984)
34. Gibson, Q.H., Regan, R., Elber, R., Olson, J.S., Carver, T.E.: Distal pocket residues affect picosecond ligand recombination in myoglobin. An experimental and molecular dynamics study of position 29 mutants. J. Biol. Chem. **267**, 22022–22034 (1992)
35. Schotte, F., Soman, J., Olson, J.S., Wulff, M., Anfinrud, P.A.: Picosecond time-resolved X-ray crystallography: probing protein function in real time. J. Struct. Biol. **147**, 235–246 (2004)
36. Li, T., Quillin, M.L., Phillips Jr., G.N., Olson, J.S.: Structural determinants of the stretching frequency of CO bound to myoglobin. Biochemistry **33**, 1433–1446 (1994)
37. Nienhaus, K., Deng, P., Kriegl, J.M., Nienhaus, G.U.: Structural dynamics of myoglobin: Spectroscopic and structural characterization of ligand docking sites in myoglobin mutant L29W. Biochemistry **42**, 9633–9646 (2003)
38. Brunori, M., Cutruzzola, F., Savino, C., Travaglini-Allocatelli, C., Vallone, B., Gibson, Q.H.: Structural dynamics of ligand diffusion in the protein matrix: A study on a new myoglobin mutant Y(B10) Q(E7) R (E10). Biophys. J. **76**, 1259–1269 (1999)
39. Nienhaus, K., Ostermann, A., Nienhaus, G.U., Parak, F.G., Schmidt, M.: Ligand migration and protein fluctuations in myoglobin mutant L29W. Biochemistry **44**, 5095–5105 (2005)
40. Brunori, M., Vallone, B., Cutruzzola, F., Travaglini-Allocatelli, C., Berendzen, J., Chu, K., Sweet, R.M., Schlichting, I.: The role of cavities in protein dynamics: crystal structure of a photolytic intermediate of a mutant myoglobin. Proc. Natl. Acad. Sci. U. S. A. **97**, 2058–2063 (2000)
41. Kriegl, J.M., Bhattacharyya, A.J., Nienhaus, K., Deng, P., Minkow, O., Nienhaus, G.U.: Ligand binding and protein dynamics in neuroglobin. Proc. Natl. Acad. Sci. U. S. A. **99**, 7992–7997 (2002)
42. Nienhaus, K., Kriegl, J.M., Nienhaus, G.U.: Structural dynamics in the active site of murine neuroglobin and its effects on ligand binding. J. Biol. Chem. **279**, 22944–22952 (2004)
43. Vallone, B., Nienhaus, K., Brunori, M., Nienhaus, G.U.: The structure of murine neuroglobin: novel pathways for ligand migration and binding. Proteins **56**, 85–92 (2004)
44. Vallone, B., Nienhaus, K., Matthes, A., Brunori, M., Nienhaus, G.U.: The structure of carbonmonoxy neuroglobin reveals a heme-sliding mechanism for control of ligand affinity. Proc. Natl. Acad. Sci. U. S. A. **101**, 17351–17356 (2004)
45. Nienhaus, G.U., Chu, K., Jesse, K.: Structural heterogeneity and ligand binding in carbonmonoxy myoglobin crystals at cryogenic temperatures. Biochemistry **37**, 6819–6823 (1998)
46. Alben, J.O., Beece, D., Bowne, S.F., Doster, W., Eisenstein, L., Frauenfelder, H., Good, D., McDonald, J.D., Marden, M.C., Moh, P.P., Reinisch, L., Reynolds, A.H., Shyamsunder, E., Yue, K.T.: Infrared spectroscopy of photodissociated carboxymyoglobin at low temperatures. Proc. Natl. Acad. Sci. U. S. A. **79**, 3744–3748 (1982)
47. Yang, F., Phillips Jr., G.N.: Crystal structures of CO-, deoxy- and met-myoglobins at various pH values. J. Mol. Biol. **256**, 762–774 (1996)
48. Vojtechovsky, J., Chu, K., Berendzen, J., Sweet, R.M., Schlichting, I.: Crystal structures of myoglobin-ligand complexes at near-atomic resolution. Biophys. J. **77**, 2153–2174 (1999)
49. Lim, M., Jackson, T.A., Anfinrud, P.A.: Ultrafast rotation and trapping of carbon monoxide dissociated from myoglobin. Nat. Struct. Biol. **4**, 209–214 (1997)
50. Kriegl, J.M., Nienhaus, K., Deng, P., Fuchs, J., Nienhaus, G.U.: Ligand dynamics in a protein internal cavity. Proc. Natl. Acad. Sci. U. S. A. **100**, 7069–7074 (2003)
51. Lehle, H., Kriegl, J.M., Nienhaus, K., Deng, P., Fengler, S., Nienhaus, G.U.: Probing electric fields in protein cavities by using the vibrational Stark effect of carbon monoxide. Biophys. J. **88**, 1978–1990 (2005)

52. Nienhaus, K., Olson, J.S., Franzen, S., Nienhaus, G.U.: The origin of Stark splitting in the initial photoproduct state of MbCO. J. Am. Chem. Soc. **127**, 40–41 (2005)
53. Springer, B.A., Sligar, S.G.: High-level expression of sperm whale myoglobin in *Escherichia coli*. Proc. Natl. Acad. Sci. U. S. A. **84**, 8961–8965 (1987)
54. Nienhaus, K., Lamb, D.C., Deng, P., Nienhaus, G.U.: The effect of ligand dynamics on heme electronic transition band III in myoglobin. Biophys. J. **82**, 1059–1067 (2002)
55. Young, R.D., Frauenfelder, H., Johnson, J.B., Lamb, D.C., Nienhaus, G.U., Phillip, R., Scholl, R.: Time- and temperature dependence of large-scale conformational transitions in myoglobin. Chem. Phys. **158**, 315–328 (1991)
56. Johnson, J.B., Lamb, D.C., Frauenfelder, H., Müller, J.D., McMahon, B., Nienhaus, G.U., Young, R.D.: Ligand binding to heme proteins. VI. Interconversion of taxonomic substates in carbonmonoxymyoglobin. Biophys. J. **71**, 1563–1573 (1996)
57. Parak, F., Heidemeier, J., Nienhaus, G.U.: Protein structural dynamics as determined by Mössbauer spectroscopy. Hyperfine Interact. **40**, 147–158 (1988)
58. Chu, K., Ernst, R.M., Frauenfelder, H., Mourant, J.R., Nienhaus, G.U., Philipp, R.: Light-induced and thermal relaxation in a protein. Phys. Rev. Lett. **74**, 2607–2610 (1995)
59. Berendzen, J., Braunstein, D.: Temperature-derivative spectroscopy: a tool for protein dynamics. Proc. Natl. Acad. Sci. U. S. A. **87**, 1–5 (1990)
60. Mourant, J.R., Braunstein, D.P., Chu, K., Frauenfelder, H., Nienhaus, G.U., Ormos, P., Young, R.D.: Ligand binding to heme proteins: II. Transitions in the heme pocket of myoglobin. Biophys. J. **65**, 1496–1507 (1993)
61. Ehrenstein, D., Nienhaus, G.U.: Conformational substates in azurin. Proc. Natl. Acad. Sci. U. S. A. **89**, 9681–9685 (1992)
62. Lamb, D.C., Nienhaus, K., Arcovito, A., Draghi, F., Miele, A.E., Brunori, M., Nienhaus, G.U.: Structural dynamics of myoglobin: ligand migration among protein cavities studied by Fourier transform infrared/temperature derivative spectroscopy. J. Biol. Chem. **277**, 11636–11644 (2002)
63. Nienhaus, K., Maes, E.M., Weichsel, A., Montfort, W.R., Nienhaus, G.U.: Structural dynamics controls nitric oxide affinity in nitrophorin 4. J. Biol. Chem. **279**, 39401–39407 (2004)
64. Phillips Jr., G.N., Teodoro, M.L., Li, T., Smith, B., Olson, J.S.: Bound CO is a molecular probe of electrostatic potential in the distal pocket of myoglobin. J. Phys. Chem. B **103**, 8817–8829 (1999)
65. Ray, G.B., Li, X.-Y., Ibers, J.A., Sessler, J.L., Spiro, G.S.: How far can proteins bend the FeCO unit? Distal polar and steric effects in heme proteins and models. J. Am. Chem. Soc. **116**, 162–176 (1994)
66. Vogel, K.M., Kozlowski, P.M., Zgierski, M.Z., Spiro, T.G.: Determinants of the FeXO (X = C, N, O) vibrational frequencies in heme adducts from experiment and density functional theory. J. Am. Chem. Soc. **121**, 9915–9921 (1999)
67. Müller, J.D., McMahon, B.H., Chien, E.Y., Sligar, S.G., Nienhaus, G.U.: Connection between the taxonomic substates and protonation of histidines 64 and 97 in carbonmonoxy myoglobin. Biophys. J. **77**, 1036–1051 (1999)
68. Nienhaus, K., Nienhaus, G.U.: A spectroscopic study of structural heterogeneity and carbon monoxide binding in neuroglobin. J. Biol. Phys. **31**, 417–432 (2005)
69. Bredenbeck, J., Helbing, J., Nienhaus, K., Nienhaus, G.U., Hamm, P.: Multidimensional ultrafast spectroscopy special feature: Protein ligand migration mapped by nonequilibrium 2D-IR exchange spectroscopy. Proc. Natl. Acad. Sci. U. S. A. **104**, 14243–14248 (2007)
70. Campbell, B.F., Chance, M.R., Friedman, J.M.: Linkage of functional and structural heterogeneity in proteins: dynamic hole burning in carboxymyoglobin. Science **238**, 373–376 (1987)
71. Ormos, P., Szaraz, S., Cupane, A., Nienhaus, G.U.: Structural factors controlling ligand binding to myoglobin: a kinetic hole-burning study. Proc. Natl. Acad. Sci. U. S. A. **95**, 6762–6767 (1998)
72. Brucker, E.A., Olson, J.S., Ikeda-Saito, M., Phillips Jr., G.N.: Nitric oxide myoglobin: crystal structure and analysis of ligand geometry. Proteins **30**, 352–356 (1998)